Ultrasensitive in-vitro monitoring of monoamine neurotransmitters from dopaminergic cells

Mohammed Y. Emran [a], Mohamed A. Shenashen [a], Moataz Mekawy [a], Ahmed M. Azzam [a], Naeem Akhtar [a], Hassenien Gomaa [a], Mahmoud M. Selim [b], Ahmed Faheem [c], Sherif A. El-Safty [a,d,*]

[a] National Institute for Materials Science (NIMS), Research Center for Functional Materials, 1-2-1 Sengen, Tsukuba-shi, Ibaraki-ken, 305-0047, Japan
[b] Department of Mathematics, Al-Aflaj College of Science and Human Studies, Prince Sattam Bin Abdulaziz University, Al-Aflaj 710-11912, Saudi Arabia
[c] School of Pharmacy and Pharmaceutical Sciences, Faculty of Health Sciences and Wellbeing, University of Sunderland, Sunderland, SR1 3SD, UK
[d] Faculty of Engineering and Advanced Manufacturing, University of Sunderland, Sunderland SR6 0DD, UK

Abstract

The design of biosensing assay of monoamine neurotransmitters (MANTs) such as epinephrine (Ep), norepinephrine (NE), and dopamine (DA), as well as the monitoring of these MANTs released from dopaminergic cells, are of particular interest. Electrochemical sensors based on the novel construction of nickel oxides (NiO) were fabricated and employed for electrochemical screening of MANTs. A novel NiO-lacy flower-like (NLF) geometrical structure with semi-spherical head surfaces connected with a trunk as an arm was achieved. The designed semi-spherical head associated with abundant and the well-dispersed tubular branches with needle-like open ends might lead to the creation of vascular vessels for facile diffusion and suitable accommodation of the released MANTs throughout active and wide-surface-area coverage, multi-diffusive pores, and caves with connective open macro-/meso-windows along the entire top-view nanoneedles of lacy flower head and trunk. These electrode surfaces possess high-index catalytic site facets associated with the formation of ridges/defects on {110}-top-cover surface dominants for strong binding, fast response, and signaling of MANTs. The NLF- modified electrode enabled high sensitivity for MANTs and a low limit of detection of 6 nM. Ultrasensitive in-vitro monitoring of DA released from dopaminergic cells (such as PC12) was realized. The NLF electrode was used to detect MANTs from its sources (PC12), and it could be used for clinical diagnosis.

1. Introduction

Monoamine neurotransmitters (MANTs), such as dopamine (DA), norepinephrine (NE), and epinephrine (Ep), play a key role in the endocrine and central nervous systems. Fluctuation levels of MANTs are a result of some neurological or immunological diseases, such as Parkinson's disease, human immunodeficiency virus infection, and schizophrenia [1–3]. DA acts as a precursor of Ep and NE, plays a key role in movements, and can be used as a cardiac stimulant and in most potent vasopressin drugs [1–3]. DA and Ep are used to treat some diseases, such as allergy, asthma, cardiac arrhythmias, and infarction [4]. MANTs have a similar chemical structure, and they are often present in biological samples. Therefore, fabrication of an efficient electrochemical biosensor to monitor and determine MANTs in their receptors or resources is clinically needed.

Several techniques such as chromatography [5,6], mass spectroscopy [7], fluorescence [8], and electrochemical approaches [9,10] have been used to detect MANTs. Most of these techniques have the following characteristics: i) need highly equipped machines, ii) time-consuming, iii) induce excessive costs, iv) required highly trained technicians, v) can be used in-vitro/in-vivo, and vi) adopt sophisticated procedures. By contrast, electrochemical methods are sensitive approaches for MANT detection [9–12]. Electrochemical techniques are more widely used for monitoring MANTs because they do not require pretreatment of samples, have a fast response, allow on-site detection, and may be performed in situ [13–17].

Several reports have shown the electrochemical responses of DA, such as modified electrodes with 3D nitrogen-doped graphene on Ni foam electrode, graphene nanosheet/SnO_2 nanocomposite, 3D interpenetrating graphene electrode,

* Corresponding author.
E-mail addresses: doneSherif.ELSAFTY@nims.go.jp, sherif.el-safty@sunderland.ac.uk (S.A. El-Safty).

imprinted poly(nicotinamide)/CuO, graphene, N-doped carbon dots (CDs), N-doped graphene/MnO, cibacron blue/poly- 1,5-diaminonaphthalene, and K^+-induced DA released from dopaminergic cells (PC12) by ethylenediaminetetraacetic acid (EDTA)-immobilized polydiaminonaphthalene (pDAN)/graphene oxide (GO)/gold nanoparticles (AuNPs) [11–18]. Electrochemical detection of Ep by using various modified electrodes, such as electrochemically pretreated glassy carbon electrodes (GCEs) [19], carbon fiber microelectrodes [20], polymer-film-modified GCEs [20–22], and other modified electrode based on functionalized substrate [23–25], has been reported. The sensitivities and linear ranges of all the methods using different modified electrodes are indicated in Table S1, and all of them have low comparable detection limits. Simultaneous detection of two or three types of MANTs is difficult because they exhibit the same oxidation-reduction mechanism.

Fabrication of modified electrodes based on metal-oxide nanomaterials, such as CuO, NiO, TiO_2 and Co_3O_4, is widely considered because of their good biological compatibility, large surface area, and special physical and chemical properties [26–34]. NiO is a transition metal oxide that has received considerable attention in many applications, such as catalysts, lithium-ion batteries, and fuel cells, because of its intrinsic properties considered as antiferromagnetic materials, easy fabrication, building of novel construction with abundant active sites, highly efficient electrocatalyst, and good electrochemical conduction [35–40]. Although many synthetic approaches can produce porous NiO and magnetism, achievement of a simple and feasible method for designing mesostructured NiO with a controlled morphology is highly desirable and remains a great challenge to material scientists.

In this study, a modified electrode based on the new design of NiO for monitoring MANTs was assembled. The controlled NiO-lacy flower-like (NLF) morphology expressed the electrode design, which was similar to a lacy flower with a semi-round architecture connected by a trunk. The designed NLF surface was like a jagged surface with thick tubular pipes that spread with unity and homogeneity over the semi-round flower head surface. The designed NLF possessed intrinsic features, which play key roles in its electrocatalytic characteristics, such as active and wide-surface-area coverage, multi-diffusive pores, and caves with connective open macro-/meso-windows along the entire top-view nanoneedles of the NLF head and trunk. The actively catalytic surface of the modified electrode assembled with the designed NLF showed highly sensitive, selective, and fast responses of MANTs. The NLF-modified electrode provided highly sensitive detection of DA secreted from living cells under K^+ stimulation with low cytotoxicity and high biocompatibility. Sensitive monitoring of MANTs from dopaminergic cells enabled the potential use of our biosensing assay for clinical diagnosis of schizophrenia, Alzheimer's, and Parkinson's diseases.

2. Experimental

2.1. Synthesis of NLF

A new morphological NiO was synthesized by one-pot hydrothermal synthetic approach. ($Ni(NO_3)_2 \cdot 6H_2O$) (1 mM) was dissolved in a 100 mL volumetric flask containing 20 mL of deionized water and was stirred until it dissolved at room temperature. $(NH_4)_2HPO_4$ solution (15 mL of 1 mM) in Milli-Q water was added to the above solution dropwise with continuous stirring. The prepared solution was transferred into a 100-mL Teflon-lined stainless-steel autoclave, sealed, and maintained at 160 °C for 8 h. After the required time, a green precipitate was retrieved and rinsed with ultrapure water/absolute ethanol to remove soluble impurities. The NLF was dried in an oven at 80 °C and annealed at 400 °C for 4 h.

2.2. Working electrode designing and formation

The NLF was dispersed in Milli Q water with concentration 5 mg/ml at room temperature and sonicated for 4 h for complete dispersion and unit formations. Thin films of NLF were fabricated by uniformly spreading 20 J-L solution of NLF onto the conducting surface of ITO glass substrate (2 cm × 1 cm). To control the exposed surface area of ITO substrate and for better electrical contact a definite area (1 cm × 1 cm) of the ITO electrode substrate were masked prior to the deposition. This process was repeated 3 times; the resulting electrode was dried overnight at room temperature, followed by washing with deionized water to remove any unbound particles.

2.3. Cell culture and in vitro study

The PC12 cell line was obtained from PC12 (ATCC® CRL1721™) and was cultured by incubation under 5% CO_2 at 37 °C in Dulbecco's Modified Eagle's Medium (DMEM) containing 10% fetal bovine serum (FBS), and 10% horse serum. The culture medium was replaced every 2–3 day.

For cells visualization experiments using (NLF), cells were seeded in 6 well-plate under 2×10^6Cells/ml. To enhance extracellular dopamine release, a desired amount of 20 mM KCl solution was added, kept in a humid chamber under 5% CO_2 at 37 °C for 15 min followed by thoroughly washing using Dulbecco's Phosphate Buffered Saline (DPBS). A desired amount of NLF (20 J-g/ml) was added to each well, incubated in a humid chamber for additional 30 min under 5% CO_2 at 37 °C followed by thoroughly washing using DPBS. Nuclear counter-staining was carried out using 0.1 J-g/ml of 4′, 6-diamidino-2-phenylindole (DAPI) in PBS for 10 min. Finally, confocal microscopy measurements were observed using Leica TCS SPE5 X machine

2.4. Cytotoxicity and cell viability

The cytotoxicity of NLF was investigated by Cell Counting Kit-8 (CCK-8) assay. The cells (5×10^3 cells/mL) were seeded onto 96-well microplates to a total volume of 100 J-L/well and maintained at 37 °C in a 5% CO_2/95% air incubator for 24 h. Then, NLF (10 J-L) with different concentrations were added (10, 20, 50 and 100 J-g/ml), and incubated for 24 h. The CCK-8 solution (10 J-L, 5 mg/ml) was added into each well and incubated for another 2–4 h in the CO_2 incubator. Then measure at absorbance of 450 nm using a microplate reader

3. Results and discussions

The controlled morphology of NiO architecture was synthesized by hydrothermal treatment after addition of $(NH_4)_2HPO_4$ as shown in Scheme S1. The PO_4^{3-} anions act as morphology directing agent for controlled designing of NiO-lacy flower like. The formation of NiO-lacy flower like depends on the presence of ammonia and water, producing OH^- anions, which directly reacts with a Ni^{2+} cation to form $Ni(OH)_2$. Phosphate anions and ammonium cations play the key role for the controlled design and enhanced the crystal growth of NiO. The self-directing formation of NLF was formed after prolonged time with the supporting of PO_4^{3-} anions. Controlled design of NiO which is like a lacy flower with semi-spherical dense head and connected by a trunk was formed.

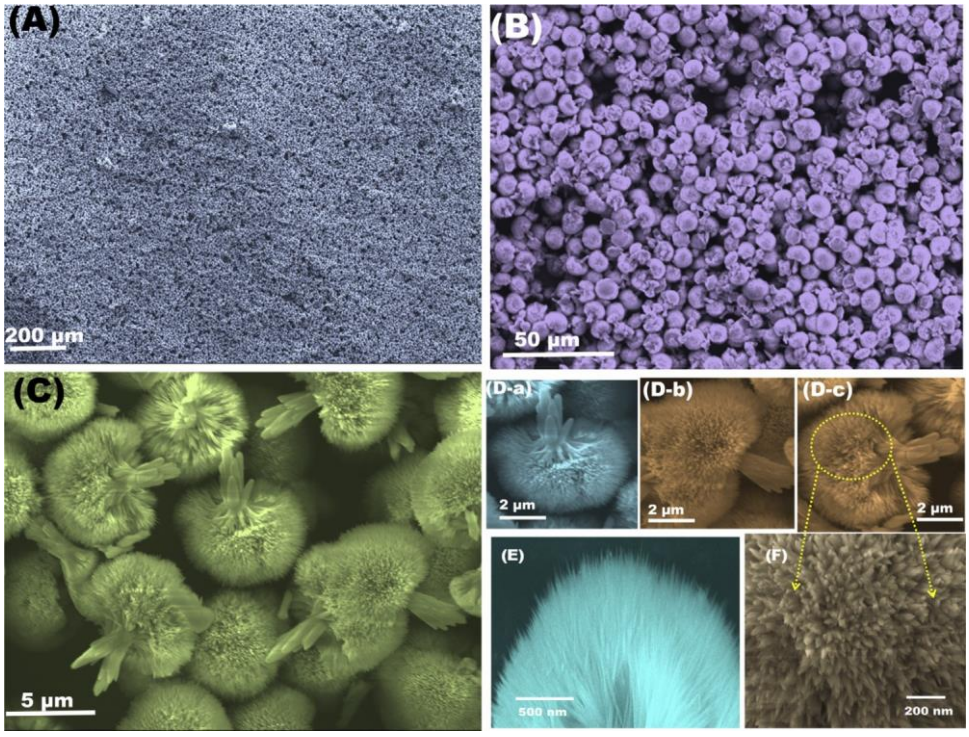

Fig. 1. A & B) The FE-SEM of NLF deposited at the ITO substrate surface is captured. C) High magnification of FE-SEM of NLF, which present the morphological shape of controlled design NiO–lacy flower like. Da-Dc) The FE-SEM of different NLF position architectures and F) high magnification of small section at NLF-head reflects the head surface morphology, which consists of nanoneedles spread from the inner surface to outer surface.

3.1. Surface features of NLF

Field-emission scanning electron microscopy (FE-SEM) was used to investigate the morphology of the synthesized material and explore the surface features. Fig. 1(A–C) shows the formation of a thin film from NLF at the ITO surface. The NLF morphological construction is formed from one head connected by a trunk like an arm. Homogeneous and uniformly construction of NLF is clearly shown in Fig. 1(A and B) with semi-spherical head and uniformed trunk with average head size from 3 to 4 J-m and 1.5–2 J-m for its trunk. The FE-SEM of the NLF focused on different point of view, including the back, front of the head, and side positions. The NLF-geometry shows the stability and unity of single head aligned vertically by a trunk in various positions as shown in Fig. 1(Da–Dc). The NLF head explores its specific features, in which the head architecture revealed like semi-spherical head with a jagged surface. The designed semi-spherical head composed of abundant and well-dispersed tubular branches, open-ends and covering the head surface with uniformity and homogeneity as presented in Figs. 1(E and F)(Scheme 1).

High-angle annular dark field scanning transmission electron microscopy (HAADF-STEM) micrographs (Fig. 2) can provide the architecture of NLF, which is like a lacy flower with semi-spherical open flower surface and branched by a trunk like an arm. Fig. 1(A-C) shows low and high magnification of HAADF-STEM from a cross-section of the NLF head. The head shows a unique morphology, which is like a jagged surface formed from well dispersed branched tubes like a needles spread out from inner to the outer surface with perpendicular alignment to the main head. The average size of the needles is approximately 15 nm as shown in Fig. 2C. The head architecture with relevant morphology provides the nature of catalytic active sites which works deeply during electrolyte diffusion at the surface of NLF. Focused ion beam (FIB) system was used to trim the thickness of the head of NLF surface using variable beam intensity until the thickness was 100 nm. Fig. 2 (D-a–D-d) shows a high magnification of HAADF-STEM, which reflects the smooth surface, the high crystalline order of NLF formed with high index {110-crystal plane with $d_{\{11\}} = 2.41$ Å, and the pores distributed deeply at nanoneedle surface. Confirmation from ED resolution of low and high index lattice planes of (− 220), (2–20), (002), and (00–2)
fringing around the bottom {110}-principle zone-dominant plan is shown in Fig. 2A (inset). The elemental mapping of NLF reflects the unity dispersion of Ni and O at its surface and provides the chemical formation as shown in Fig. 2(E-a and E-b). The NLF surfaces fully configured by FE-SEM and HAADF-STEM, and outline the structure and morphological features, and obtain the nanostructure attributed to the nanoneedles at its surface and highly crystalline order with dominant {110}-crystal plane.

Surface nature and atomic configuration of NiO around the {110}-crystal plane provide the interaction of MANTs at the modified electrode surface such as rapid electron transport and strong binding with the target molecules as presented in Fig. 3A. The NLF surface structure domain mesoporous framework construction around the {110}-crystal plane increases the actively energetic surface coverage for facile diffusion. Fig. 3B shows the electronic configuration of Ni^{2+} and O^{2-} at the top surface around the axial {110}-crystal plane, and provides charge-rich iso-surfaces. Fig. 3B and C show the atomic single-layer and double-layer-exposed for configuration of {110} crystal surface plane. Furthermore, Fig. 3D and E illustrate the {110}-top-surface around the double-layer surfaces, which provide high-energy electron surfaces formed along the entire NiO crystal structure directed along the exposed surface. The 4-Ni^{2+}-top surfaces (Fig. 3E) enhance the electrocatalytic activity of Ni^{+2} with the target molecules by directly contacting with the target molecules, providing the reusability and multi-diffused open pores/cavities. This phenomenon directly influenced the sensitivity and selectivity, enabling several reuses/cycling of the catalysts.

Surface nature is provided by N_2 adsorption-desorption isotherms. Fig. S1A shows the N_2 adsorption-desorption isotherm, which identified as type IV with an H1 hysteresis loop [41–43].

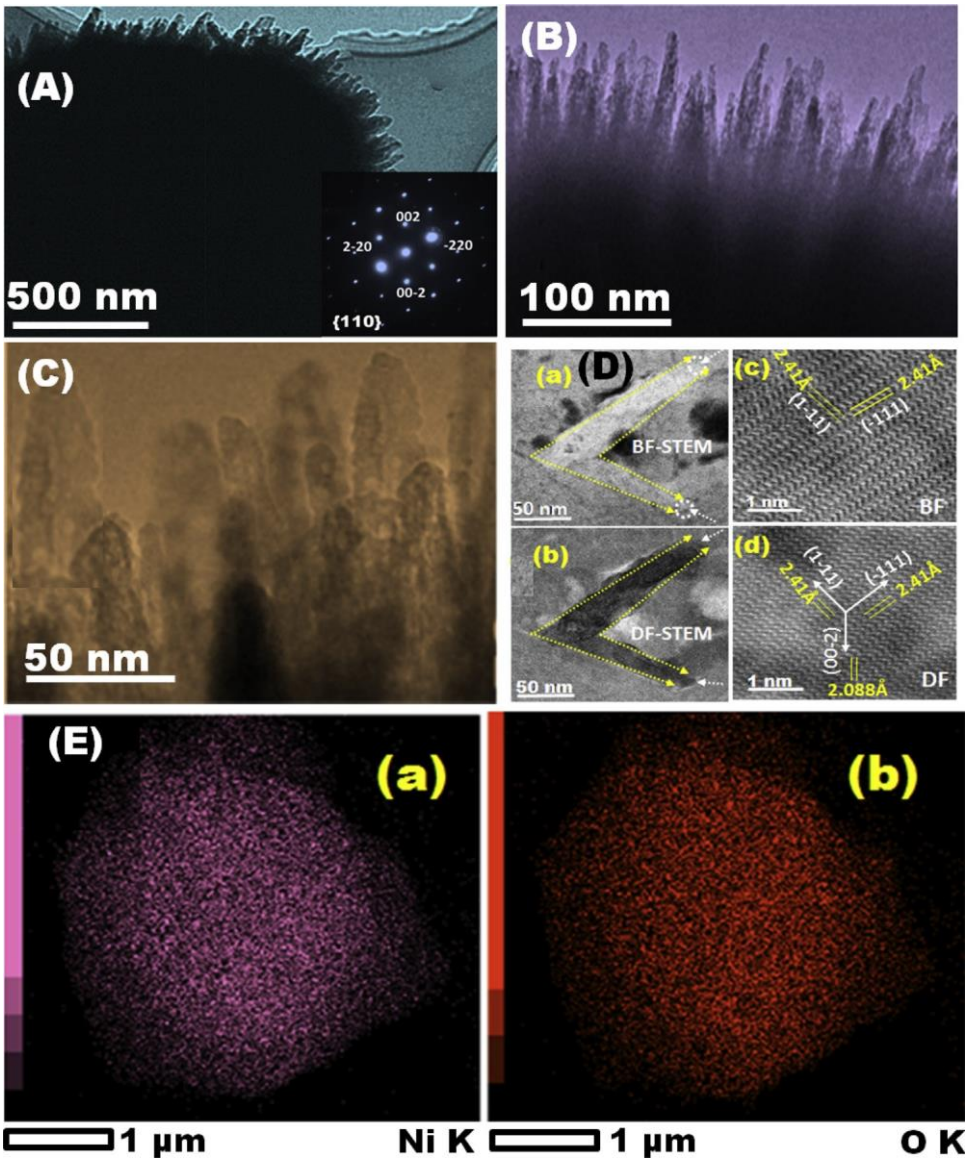

Fig. 2. A&B) The HAADF–STEM micrograph cross-section of the NLF head. C&D) Low-and high magnification of HAADF–STEM micrographs of the head needle ends illustrate a smooth surface with definite pores which clearly on Ea − Ed and degree crystalline surface where the surface obtain the high crystalline degree of nucleus NiO with $d_{\{110\}} = 2.41$ Å with dominant *{110}* plane of interfaces. Inset of A) The corresponding electron diffraction (ED-STEM) pattern of NLF around *{110}*-crystal plane. E-a&E-b) The EDS mapping of NiO for atomic distribution of Ni and O, respectively.

The pores distribution is investigated by nonlocal density functional theory model (NLDF), which promotes the pore size and pore volume of the constructed NLF. As shown in the inset of Fig. S1A, two different pores size distributed at the surface of NLF and all of them are in the mesoporous range (2.72 and 13.22 nm). The NLF featured a specific surface area of $S_{BET} = 60.2\ m^2\ g^{-1}$, which is larger than nanoplatelets NiO ($20.2\ m^2\ g^{-1}$), nonporous dendritic NiO ($5.06\ m^2 g^{-1}$), and capsule-like NiO nanoparticles ($48.9\ m^2 g^{-1}$) [44–46]. Dominant mesoporous surface construction and high surface area of NLF enhance the diffusion or adsorption of the specific molecules and increase the electrocatalytic activity. The crystal structure and degree of crystalline surface of NLF are investigated using wide-angle X-ray diffraction patterns. Fig. S1 B shows sharp and well-resolved diffraction peaks for the NiO sample centered at at37.2 ° , 43 ° , 63 ° , 75.5 ° , and 79.6 corresponds to the (111), (200), (220), (311), and (222) planes, respectively. The NLF exhibits face-centered cubic (fcc) lattice structure and confirmed by matching with JCPDS no. 01-089-5881 [35,36,47]. The confirmation of pristine NiO was confirmed by Raman spectrum ranged from 460 to $1400\ cm^{-1}$ at the excitation wavelength of 532 nm as shown in Fig. S2A. The Raman spectra of NLF showed a vibrational band at approximately $532\ cm^{-1}$ caused by one phonon corresponding to the first-order transverse optical (TO) mode. The peaks of two phonons at approximately 760 and 1085 cm^{-1} were attributed to two TO modes and two longitudinal optical modes, respectively, indicating the presence of pristine NiO [35,36]. Further confirmations of the surface components of NLF, X-ray photoelectron spectroscopy (XPS) measurements were performed. Fig. S2 B shows a wide range of XPS spectra (i.e., survey) of NiO components. Fig. S2C shows the Ni 2p spectra with the main peaks centered at 872.3 and 854.3 eV assigned to Ni 2p1 and Ni 2p3 of Ni(II) ions, respectively [35,36]. The peaks of Ni 2p and O 1 s in the NLF undergo visible shifts to low binding energy compared with pristine NiO (Fig. S2(C &D).

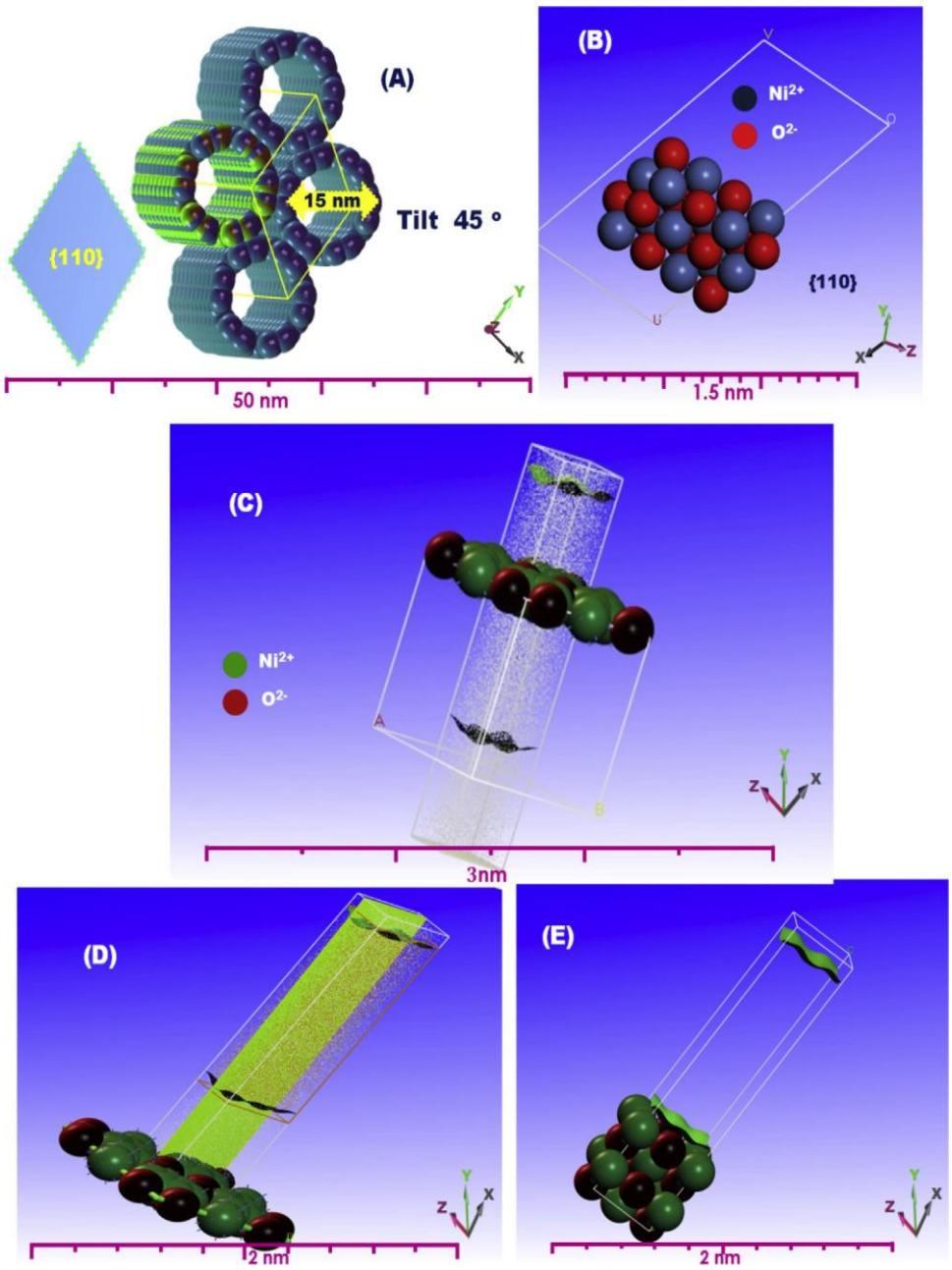

Fig. 3. (A) Mesostructured *{110}*–NiO crystal facet. (B) The atomic configuration of NiO crystal into exposed *{110}* surface plane. (C, D) High energy surfaces formed along the entire NiO crystal structure directed along *{110}* surface exposure (i.e., top (C), and bottom (D)). (E) Dense atomic configuration of Ni^{2+} and O^{2-} around *{110}*-crystal plane.

3.2. Electrochemical statements of the NLF-modified electrode

The electrochemical behavior of NLF-modified electrode was investigated using cyclic voltammetry in 0.1 M PBS (pH = 7.0) containing 0.1 mM $[Fe(CN)_6]^{3-}$ within potential range from − 0.2 V to 0.8 V (vs. Ag/AgCl) at a scan rate of 100 mV/s (Fig. S3A). The electrochemical nature, surface properties of the modified electrode, and rate of diffused ions are investigated by $[Fe(CN)_6]^{3-}$ as a redox probe [11–14]. As obtained in Fig. S3A (wine line), the peak-to-peak separation (Ep) value of the NLF-modified electrode (183 mV) is significantly lower than that of the ITO (204 mV) electrode (Fig.S3A (blue line)). These results provide that the electron transfer was affected by the fabrication of NLF at ITO electrode. The nanoscale design of NLF, novel construction and dominant mesoporous enhance the NLF nature and increase the catalytic active sites at the nanoscale surface for the Faradaic redox reaction [48–51]. The anodic and cathodic current of $[Fe(CN)_6]^{3-}$ at the NLF-modified electrode is higher than that of the bare electrode (ITO) within threefold, enforcing the high active surface area of the designed electrode.

Further confirmation of the active modified electrode surface; impedance spectroscopy measurement was performed, the semicircle diameter reflects the electron transfer resistance (Ret) of the electrode, and the line reflects the diffusion of the electroactive species [48–51]. Fig. S3B shows the typical Nyquist impedance plots of the NLF-modified electrode (wine scatter) and ITO (wine scatter) electrode in 0.1 M PBS (containing 0.1 M $[Fe(CN)_6]^{3-}$). The NLF-modified electrode exhibit a short semicircle diameter at high frequency, and a relative small Ret. From the fitting circuit the Ret for ITO = 876.9 Q, while for NLF/ITO = 380 Q. The semicircle of the

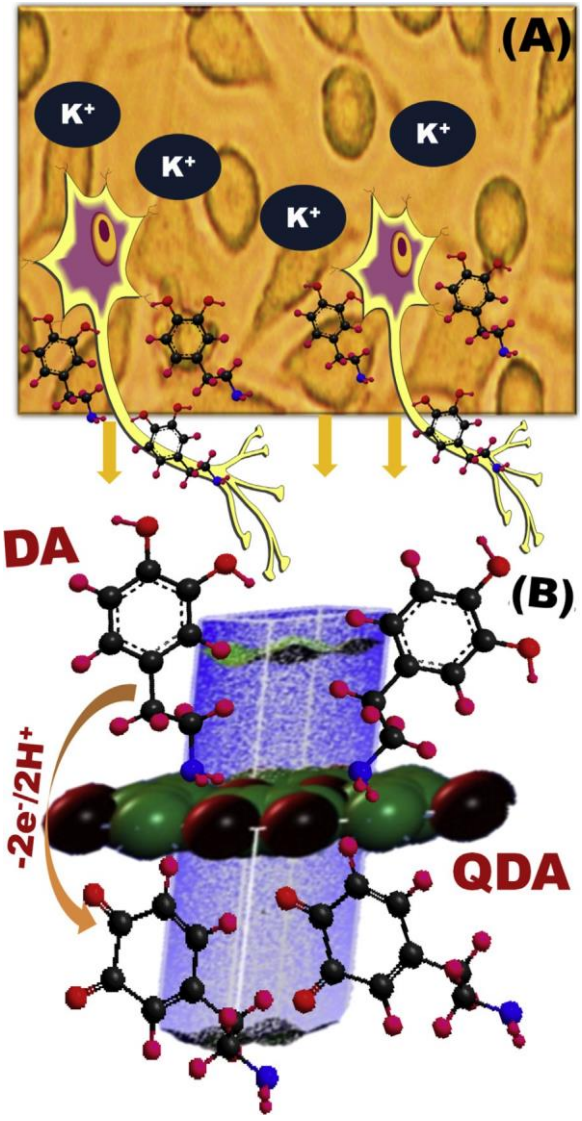

Scheme 1. A) Confocal microscope image of PC12 incubated with 20 mM KCl for 30 min and producing extracellular MANTs (i.e dopamine). B) Electrochemical biosensing of DA release form PC12 by NLF-modified electrode at the direct contact surface of the *{110}*-crystal plane and formation QDA with losing of $2e^-$ /$2H^+$.

NLF-modified electrode obtains a further decrease in extremely low Ret value and high conductivity. These results suggest that the designed NLF enhances the electron-transport efficiency of the ITO-modified electrode surface [48–51]. Our finding promotes that the NLF with (i) geometric shape lacy flower with a head and trunk and (ii) formation of a 15–20 nm nanoneedles at the top of head surface, and iii) mesostructured with high-index lattice fringes along the principal *{110}* plane may lead to the creation of effective electrocatalyst surface for electron diffusion and mass transport pathway.

The electrooxidation of MANTs at the surface of NLF- modified electrode was investigated using differential pulse voltammetry (DPV) in the presence and absence of the target molecules in 0.1 M PBS pH = 7, pulse height of 60 mV, pulse distance of 200 ms, pulse width of 25 ms, and step height of 5 mV. A well-resolved DPV peaks centered at 0.12, 0.17, and 0.21 V for 5 J-M Ep, 5 J-M NE, and 5 J-M DA, respectively as shown in Fig. 4 (A–C). The electrooxidation of MANTs such as Ep, NE, and DA because of the oxidation form formation of o-quinone with losing of $2e^-$ /$2H^+$. Highly current response upon addition of MANTs at low concentrations (5 J-M) during the comparison between 0 and 5 J-M are observed at honestly applied potential. This result is related to the high electrocatalytic performance of NLF-modified electrode throwing its surface (Figs. 4(A–C)). High surface area and dense active sites expose and induce the electrocatalytic oxidation of MANTs with easy molecular diffusion and high electron transfer at the NLF-modified electrode. Highly electrocatalytic activity and easily diffused molecules at the surface of the NLF-modified electrode are the key roles for enhancing the peak potentials of MANTs. The difference between the oxidation peak potential (ΔE) between Ep and NE ($\Delta E_{EP-NE} = 0.05$ V), NE and DA ($\Delta E_{NE-DA} = 0.04$ V), and Ep and DA ($\Delta E_{Ep-DA} = 0.9$ V) strongly support the highly electrocatalytic, and easy diffusion of MANTs at the surface of the modified electrode. One- step signaling of two or three forms of MANTs shows a broad DPV peak. Fig. S4 (A-C) shows a broad DPV peak upon screening of 20 J-M of NE and DA. The same behavior was observed for 20 J-M of Ep and NE. a wide and high DPV peak is obtained upon screening of the three molecules in one pot (5 J-M of Ep, NE, and DA). All the neurotransmitters have the same oxidation mechanism but a slight difference in the chemical structure, so they overlapped and broaden the DPV peak.

3.3. Sensitive and selective screening of MANTs

Validation of sensitive detection of MANTs (Ep, NE, and DA) was performed at the NLF-modified electrode in 0.1 M PBS, pH = 7.0 using DPV at a pulse height of 60 mV, the pulse width of 25 ms, pulse distance of 200 ms, and a step height of 5 mV. The oxidation peak currents of Ep increased with increasing its concentration ranging from 1 J-M to 32 J-M (Fig. S5A). A linear relationship was revealed from plotting the concentration of Ep versus the oxidation peak current with regression equation I(J-A) = 0.91 + 0.034[Ep] (J-M) ($R^2 = 0.87$) with repeated sample number = 3, (S/N = 3) (inset in Fig. S5A), and the detection limit was calculated to be 80 nM. The same behavior for NE and DA by adding different concentrations ranging from 1 J-M to 32 J-M for each analyte indicate the sensitivity of the designed electrode. The oxidation peak currents increased with the increasing concentration of NE and DA. From plotting the concentrations of NE and DA versus the oxidation peak currents (Fig. 5S (B&C) and its insets), a linear relationship was observed with regression equation I(J-A) = 0.82 + 0.054 [NE] (J-M) ($R^2 = 0.91$), and I(J-A) = 0.79 + 0.064 [DA] (J-M) ($R^2 = 0.89$, (S/N = 3) for NE and DA, respectively. The detection limits were calculated to be 80 and 85 nM for NE and DA, respectively.

Sensitive monitoring of MANTs at low concentrations at the NLF-modified electrode was investigated by a chronoamperometric technique in 0.1 M PBS (pH = 7) at the honestly applied potential for each target molecule. Fast and well-observed current response upon step adding of 0.5 J-M of Ep at 0.12 V provides high sensitivity of the designed electrode. From the linear relationship between the concentration versus the peak current, the regression equation is I(J-A) = 3.31 + 22.75[Ep] (J-M) ($R^2 = 0.9994$). The detection limit is 7 nM (S/N = 3) as shown in Fig. 5A and its inset. This result configures that the NLF-modified electrode has high sensitivity for Ep as compared with l-cysteine/GCE and triazole SAM/GCE as presented in Table S1 [23,24]. The same response was observed for NE and high amperometric response at 0.17 V with a step adding of 0.5 J-M. By plotting [NE] (J-M) versus I(J-A), a linear relationship was obtained with regression equation I(J-A) = 3.31 + 22.75[NE] (J-M) ($R^2 = 0.9997$). The detection limit was 6 nM (S/N = 3) as shown in Fig. 5B and its inset. Finally, monitoring of DA at NLF- modified electrode was investigated at 0.21 V. The amperometric response of DA indicates high sensitivity at low concentrations, wherein the current increased at a step adding of 0.5 J-M DA as shown in Fig. 5C. The relationship of the concentration of DA and the resulting current is linear with regression equation I(J-A) = 2.63 + 19.04[DA] (J-M) ($R^2 = 0.9993$) (S/N = 3) (Fig. 5C, inset). The detection limit

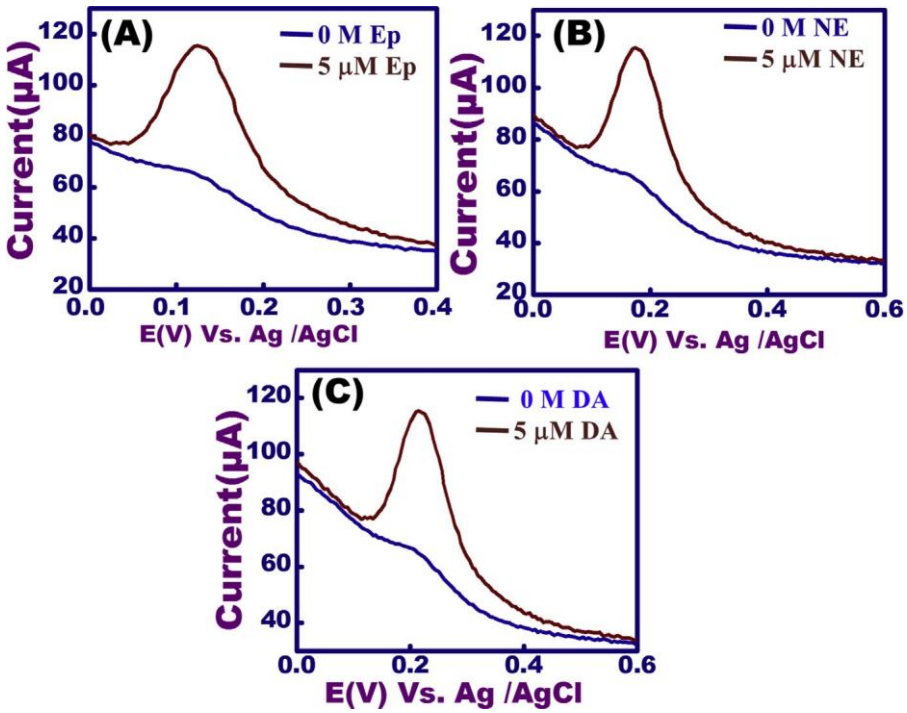

Fig. 4. The DPV of 5 J-M Ep (A), 5 J-M NE (B), and 5 J-M DA (C) at pulse height 60 mV, Pulse width 25 ms, pulse distance 200 ms and step height 5 mV on NLF − modified electrode.

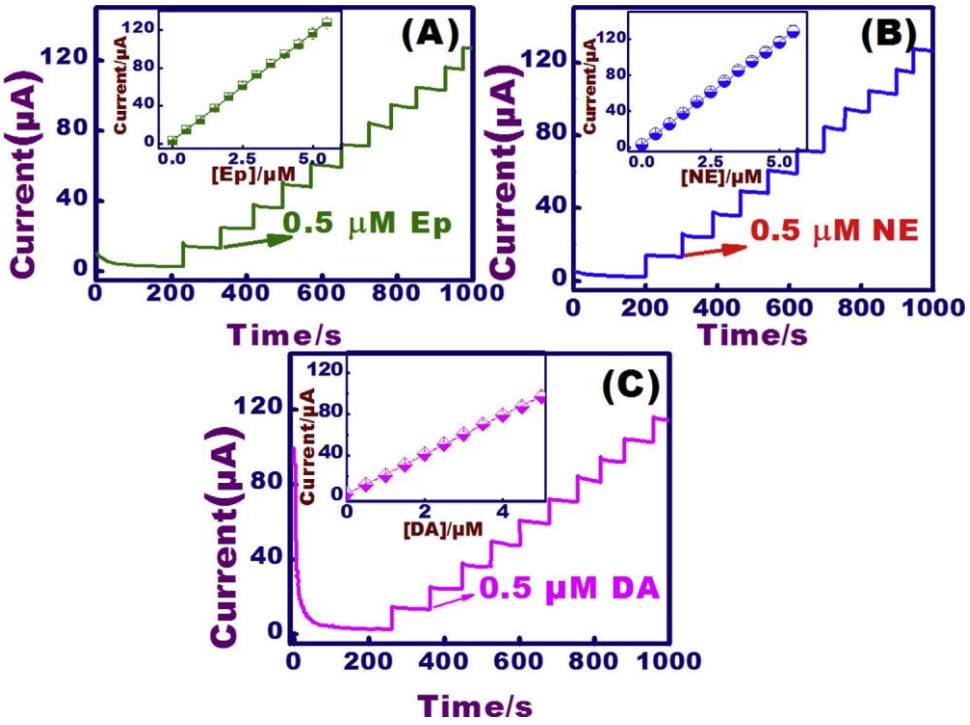

Fig. 5. The amperometric response of epinephrine (A) norepinephrine (B) and dopamine (C) with successive addition of each one from 0.5 to 5 J-M, inset the linear plot of concentration (J-M) vs the current (J-A) on NLFmodified electrode at fixed applied potential 0.12, 0.17 and 0.21 V for Ep, NE and DA, respectively.

was calculated to be 8 nM. This result provides that NLF- modified electrode is superior sensitive for DA-biosensing at low concentrations. The detection limit of NLF-modified electrode matches with the expected concentration of DA in the human plasma (0.23 J-M) and the human brain (0.02–0.2 J-M). From Table S1, NLF-modified electrode has lower detection limit compared with graphene nanosheet/SnO_2 [12], 3D reduced GO [13], N-doped graphene/MnO [16], and cibacron blue/poly-1,5-DAN [17]. Meanwhile, NLF-modified electrode has higher detection limit than molecularly imprinted poly(nicotinamide)/CuO NPs [14], N-doped CD [15], and GO/AuNPs/pDAN-EDTA [18], whereas NLF-modified electrode has higher linear range.

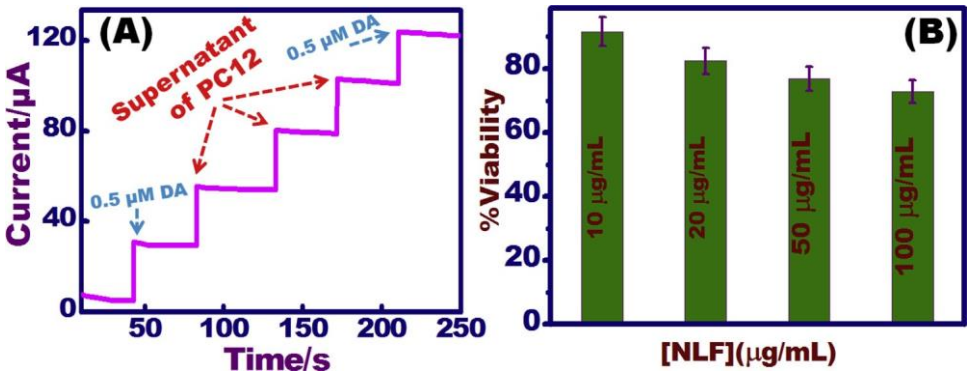

Fig. 6. A) The amperometric response of 0.5 J-M DA injected to N_2-saturated 0.1 M PBS (pH 7) at 0.21 V and continuous injection of PC12supernatant containing the released DA under 20 mM K^+ simulation on the NLF-modified electrode. B) The CCK-8 assay for cytotoxicity of various NLF concentrations (10–100 J-g/ml) of $5*10^4$ cell/mL PC12 were performed using microplate reader at 450 nm.

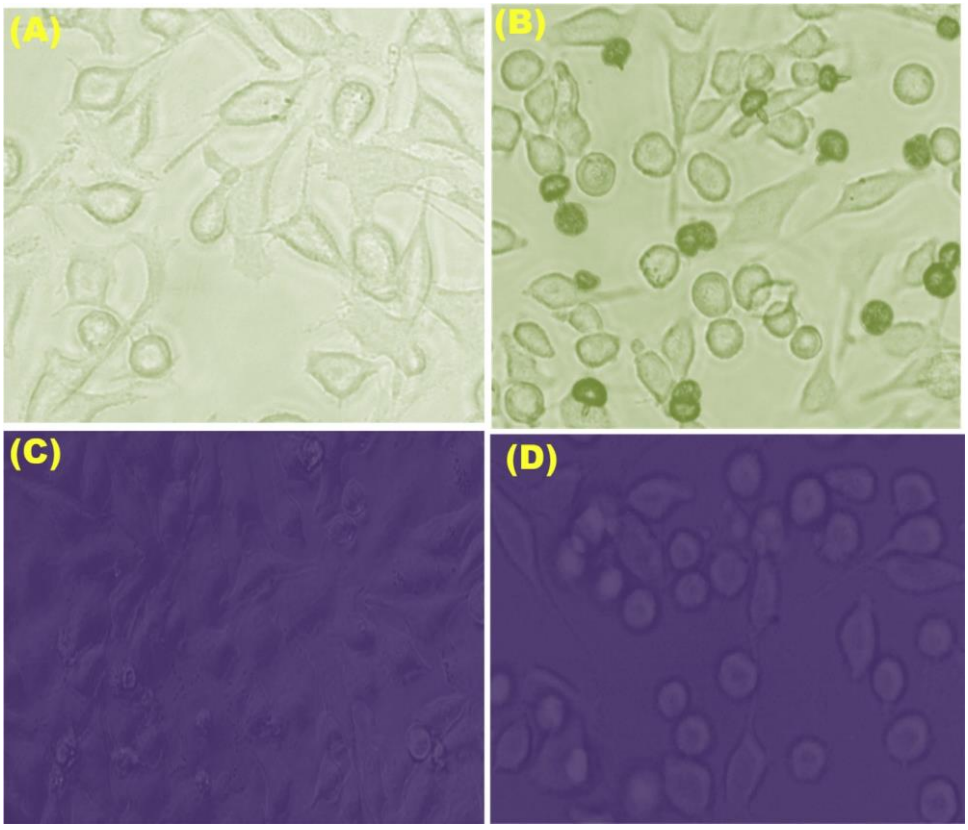

Fig. 7. Confocal microscope images recorded at excitation wavelength of 488 nm and emission wavelength at 620 nm of control PC12 cells (A) and incubation of PC12 with 20 mM KCl for 30 min (C), PC12 cells with 0.1 J-g/ml NLF for 30 min (B) and incubated PC12 +0.1 J-g/ml NLF with 30 mM KC l for 30 min (D).

3.4. In- vitro monitoring of DA released from dopaminergic cells induced by K^+

DA-secreted from neuronal cells is the key role in regulating neural mechanism and various brain functions [1,52]. In-vitro monitoring of DA-secreted from PC12 under K^+ stimulation based on the electrochemical sensor with the advanced fabrication of modified electrode is achieved. Fabrication of NLF-modified electrode for sensitive detection of DA-secreted from PC12 is performed using a different electrochemical technique such as DPV and chronoamperometry. First, we directly investigate the various concentrations of DA in 0.1 M PBS (pH 7.0) without cell addition as shown in Fig. S6A. Similarly, we observe the corresponding current peak of DA in 0.1 M PBS (pH = 7.0) + PC12 cells (2×10^6 cells/ml) induced with 20 mM K^+ along with the increasing concentration of DA (Fig. S6B). A significant increase in the current response was observed for each oxidation peak upon addition of 20 mM K^+-induced PC12 as compared to the current response of the added DA without cells as in Fig. S6C. The stimulated DA released from PC12 was monitored by the NLF-modified electrode and the actual DA concertation secreted from the cells was calculated by canceling its blank (DA addition in PBS without cells) and obtained an average current of 9.185 J-A, with (S/N = 3). By matching the current value with the obtained calibration curve, the DA concentration released from these cells was

0.34 J-M, wherein each single cell releases 0.17×10^{-6} J-M/2*10^6 cells. The DA concentration in the human plasma is 0.23 J-M, and that in the human brain is 0.02–0.2 J-M. Meanwhile, our designed electrode exhibits a high sensitivity of up to 8 nM, which agrees with the concentration levels of DA in the plasma and human brain.

Sensitive biosensor for monitoring of DA released from neuronal cell line such as PC12 was further studied using the chronoamperometric method. Fig. 6A shows significant amperometric response upon injection of 0.5 J-M DA within a few seconds on the NLF-modified electrode. The same equivalent response observed upon injection of supernatants of 1*10^6 cells/mL which contains DA released from PC12 under 20 mM K^+ stimulation, then confirmed by injection of 0.5 J-M DA. These results suggest that the reliability of the NLF − modified electrode for clinical diagnosis using different
electrochemical techniques and endorse MANTs from dopaminergic cells (PC12).

Cell Counting Kit-8 (CCK-8) was used for investigation of cell proliferation and cytotoxicity assays. The cytotoxicity of NLF was investigated upon incubation of PC12 with various concentrations at 37 ° C for 48 h. The metabolic activity of PC12 cells decreased as concentration increased (Fig. 6B). Untreated cells were acts as a control for all measurements. The NLF provides low cytotoxicity for PC12 cells, where 27% cells were lost at high concentration 200 J-g/ml and around 8% for 10 J-g/ml. Thus, NLF has no significant effect on the cell populations and provides low cytotoxicity and cell viability.

Furthermore, the biocompatibility and application of NLF for in-vitro studied; PC12 cells were visualized using laser scanning confocal microscopy measurements after confirming the active wavelength region (Fig. 7). After incubation of PC12 cells (5×10^5 cells/mL) with 0.1 J-g/ml of NLF for 4 h, then counterstaining the cells with4,6-diamidino-2-phenylindole (DAPI) as nuclear counterstaining. An in vitro model was adapted to study the interaction of NLF (20 J-g/ml) and PC12 cells (5×10^5 cells/ml) with providing its biocompatibility. The DAPI (0.1 J-g/ml) was used for PC12 cell nuclear counter-staining without incubation with NLF, which indicates the localization within the cell (Fig. 7A). Fig. 7B and D shows the co-localization and matching between NLF and DAPI counterstain under K^+ incubation, which reflects high degree of matching positivity. In addition, biocompatibility was observed after confocal microscopy visualization of the cells incubated with NLF (Fig. 7B and D) (20 J-g/ml) and control (Fig. 7 A and C), wherein no cell structure change or cytoplasm damage was observed and the micro unit of NLF was clearly obtained with cell imaging with high degree matching of biocompatibility. All these studies confirmed that the NLF can also be used as a real in vitro model for extracellular DA-sensing with high sensitivity, biocompatibility and low cytotoxicity.

3.5. Stability and reproducibility

The NLF-modified electrode reproducibility was investigated. DPV was used for this experiment under optimization conditions. The oxidation peak currents obtained from 10 J-M DA on NLF-modified electrode are tested for 5 electrodes. The relative standard deviation of the five amperometric response assays is 2.5% as evidenced by the fitting plot of the response current graphs (Fig. S7A). The reusability of the NLF-modified electrode was confirmed upon signaling of 5 different samples containing 10 J-M DA. The% RSD = 3.7 after successive monitoring of DA at the same electrode for 5 samples and every time the NLF -modified electrode washed with distilled H_2O (Fig. S7B). As a result, the reused NLF -modified electrode showed high sensing response efficiency (i.e., 98%) despite five reuses/cycles.

4. Conclusion

A simple, reliable electrode was successfully developed for sensitive detection of monoamine neurotransmitters and successful in vitro monitoring of DA released from dopaminergic cells such as PC12-induced K^+. The NLF was characterized using different techniques, confirming the structure, which is like a lacy flower with a head and trunk, wherein the head size was in the range of 3–4 J-m and the trunk size was 1.5–2 J-m. The NLF structure was stable, and the head consists of a nanoneedle at its ends and covers the entire head with an average size of 15 nm. The novel structure of NLF shows the high surface area of 60.2 $m^2 g^{-1}$ with dominant mesoporous structure, and smooth surface of nanoneedles, indicating the high sensitivity and selectivity of MANTs molecules using our designed electrode. The NLF reflects the electrocatalytic effect of the electrode surface with many active sites, easy diffusion of molecules and high electron transfer at the electrode-electrolyte interfaces. The NLF-modified electrode exerts excellent electrocatalytic activity toward MANTs in the presence of single, binary or tertiary mixture. The NLF-modified electrode shows sensing functionality in terms of high sensitivity, wide-range concentration detection, and low limit of detection up to 6 nM. The fabricated electrochemical electrode was further used for the detection of DA released from PC12-induced K^+ in biological samples. Our results show that the NLF-modified electrode successfully monitors and quantitatively detects monoamine neurotransmitters released from living cells, which can be used in clinical diagnosis. Furthermore, high biocompatibility and low cytotoxicity NLF provides a promising in vitro model for extracellular DA signaling from living cells.

Acknowledgment

We thank Dr. Hiromi Morita, staff of Nanotechnology Innovation Station, NIMS, 1-2-1 Sengen, Tsukuba 305-0047- Japan for her assistance with cell culture, cells toxicity and viability, and confocal Microscope.

Appendix A. Supplementary data

Supplementary data associated with this article can be found, in the online version, at https://doi.org/10.1016/j.snb.2017.11.156.

References

[1] J.W. Mo, B. Ogorevc, Simultaneous measurement of dopamine and ascorbate at their physiological levels using voltammetric microprobe based on overoxidized poly (1,2-phenylenediamine)-coated carbon fiber, Anal. Chem. 73 (6) (2001) 1196–1202.

[2] E. Colin-Orozco, M.T. Ramirez-Silva, S. Corona-Avendano, M. Romero-Romo, M. Palomar-Pardave, Electrochemical quantification of dopamine in the presence of ascorbic acid and uric acid using a simple carbon paste electrode modified with SDS micelles at pH 7, Electrochim. Acta 85 (2012) 307–313.

[3] R.M. Wightman, L. May, A.C. Michael, Detection of dopamine dynamics in the brain, Anal. Chem. 60 (13) (1988) 769A–779A.

[4] Y. Li, Y. Umasankar, S.M. Chen, Multiwalled carbon nanotubes with poly(NDGAChi) biocomposite film for the electro-catalysis of epinephrine and norepinephrine, Anal. Biochem. 388 (2009) 288–295.

[5] Y.S. Liu, J. Zhang, X.M. Xu, M.K. Zhao, A.M. Andrews, S.G. Weber, Capillary ultrahigh performance liquid chromatography with elevated temperature for sub-one minute separations of basal serotonin in submicroliter brain microdialysate samples, Anal. Chem. 82 (2010) 9611–9616.

[6] C.J. Ji, J. Walton, Y. Su, M. Tella, Simultaneous determination of plasma epinephrine and norepinephrine using an integrated strategy of a fully automated protein precipitation technique, reductive ethylation labeling and UPLC–MS/MS, Anal. Chim. Acta. 670 (2010) 84–91.

[7] V. Vorsa, K.F. Willey, N. Winograd, Photoionization of gas-Phase versus ion-Beam-Desorbed dopamine with femtosecond laser pulses, Anal. Chem. 71 (1999) 574–581.

[8] V. Sindelar, M.A. Cejas, F.M. Raymo, W.Z. Chen, S.E. Parker, A.E. Kaifer, Supramolecular assembly of 2,7-dimethyldiazapyrenium and cucurbit[8]uril:

a new fluorescent host for detection of catechol and dopamine, Chem. Eur. J. 11 (2005) 7054–7059.
[9] D. Brondani, C.W. Scheeren, J. Dupont, I.C. Vieira, Halloysite clay nanotubes and platinum nanoparticles dispersed in ionic liquid applied in the development of a catecholamine biosensor, Analyst 137 (2012) 3732–3739.
[10] Y.Z. Zhou, M.F. He, C.C. Huang, S.Y. Dong, J.B. Zheng, A novel and simple biosensor based on poly(indoleacetic acid) film and its application for simultaneous electrochemical determination of dopamine and epinephrine in the presence of ascorbic acid, J. Solid State Electrochem. 6 (2012) 2203–2210.
[11] X. Feng, Y. Zhang, J. Zhou, Y. Li, S. Chen, L. Zhang, Y. Ma, L. Wang, X. Yan, Three-dimensional nitrogen-doped graphene as an ultrasensitive electrochemical sensor for the detection of dopamine, Nanoscale 7 (2015) 2427–2432.
[12] Y. Ankang, Y. Xue, Y. Zhang, X. Zhang, H. Zhao, X. Li, Y. He, Z. Yuan, A simple one-pot synthesis of graphene nanosheet/SnO2 nanoparticle hybrid nanocomposites and their application for selective and sensitive electrochemical detection of dopamine, J. Mater. Chem. B. 1 (2013) 1804–1811.
[13] X. Yu, K. Sheng, G. Shi, A three-dimensional interpenetrating electrode of reduced graphene oxide for selective detection of dopamine, Analyst 139 (2014) 4525–4531.
[14] B. Li, Y. Zhou, W. Wu, M. Liu, S. Mei, Y. Zhou, T. Jing, Highly selective and sensitive determination of dopamine by the novel molecularly imprinted poly(nicotinamide)/CuO nanoparticles modified electrode, Biosens. Bioelectron. 67 (2015) 121–128.
[15] Y. Jiang, B. Wang, F. Meng, Y. Cheng, C. Zhu, Microwave-assisted preparation of N-doped carbon dots as a biosensor for electrochemical dopamine detection, J.Colloid Interface Sc. 452 (2015) 199–202.
[16] R. Chen, Y.Z. Wang, Y. Liu, J. Li, Selective electrochemical detection of dopamine using nitrogen-doped graphene/manganese monoxide composites, RSC Adv. 5 (2015) 85065–85072.
[17] A.A. Abdelwahab, H.-M. Lee, Y.-B. Shim, Selective determination of dopamine with a cibacron blue/poly-1,5-diaminonaphthalene composite film, Anal Chim. Acta. 650 (2009) 247–253.
[18] T.A. Mir, M.H. Akhtar, N.G. Gurudatt, J.-I. Kim, C.S. Choi, Y.-B. Shim, An amperometric nanobiosensor for the selective detection of K+-induced dopamine released from living cells, Biosens. Bioelectron. 68 (2015) 421–428.
[19] X. Wu, L. Mu, W. Zhang, Impedance of the electrochemical oxidation of epinephrine on a glassy carbon electrode, J. Electroanal. Chem. 352 (1–2) (1993) 295–302.
[20] Y. Sun, B. Ye, Y. Wang, X. Tang, X. Zhou, Study on the determination of neurotransmitters using poly (Neutral red) coated carbon fiber microelectrodes, Microchem. J. 58 (1998) 182–189.
[21] H.-S. Wang, D.-Q. Huang, R.-M. Liu, Study on the electrochemical behavior of epinephrine at a poly(3-methylthiophene)-modified glassy carbon electrode, J. Electroanal. Chem. 570 (2004) 83–89.
[22] H. Jeong, H. Kim, S. Jeon, Modified glassy carbon electrode by electropolymerization of tetrakis-(2-aminopheny) porphyrin for the determination of norepinephrine in the presence of ascorbic acid, Microchem. J. 78 (2004) 181–187.
[23] S.F. Wang, D. Du, Q.C. Zou, Electrochemical behavior of epinephrine at L-cysteine self-assembled monolayers modified gold electrode, Talanta 57 (4) (2002) 687–692.
[24] Y.X. Sun, S.F. Wang, X.H. Zhang, Simultaneous determination of epinephrine and ascorbic acid at the electrochemical sensor of triazole SAM modified gold electrode, Sens. Actuators B 113 (2006) 156–162.
[25] H. Fernando, T.C. Cincotto, A.M. Canevari, R.L. Campos, A.S.M. Sírgio, Simultaneous determination of epinephrine and dopamine by electrochemical reduction on the hybrid material, Analyst 139 (2014) 4634–4640.
[26] M. Knez, A. Kadri, C. Wege, U. G1osele, H. Jeske, K. Nielsch, SiO2/graphene oxide decorated with Ag nanoparticles atomic layer deposition on biological macromolecules: metal oxide coating of tobacco mosaic virus and ferritin, Nano Lett. 6 (2006) 1172–1177.
[27] P. Porta, S.D. Rossi, M. Faticanti, G.L. Minelli, I. Pettiti, L. Lisi, M. Turco, Perovskite-type oxides I. Structural magnetic, and morphological properties of LaMn1-xCuxO3 and LaCo1-xCuxO3 solid solutions with large surface area, J. Solid State Chem. 146 (1999) 291–304.
[28] M.D. Irwin, D.B. Buchholz, A.W. Hains, R.P.H. Chang, T.J. Marks, p-Type semiconducting nickel oxide as an efficiency-enhancing anode interfacial layer in polymer bulk-heterojunction solar cells, Proc. Natl. Acad. Sci. U.S.A. 105 (2008) 2783–2787.
[29] S. Cherevko, C.H. Chung, The porous CuO electrode fabricated by hydrogen bubble evolution and its application to highly sensitive non-enzymatic glucose detection, Talanta 80 (2010) 1371–1377.
[30] L. Kong, Z. Ren, N. Zheng, S. Du, J. Wu, J. Tang, H. Fu, Interconnected 1D Co3O4 nanowires on reduced graphene oxide for enzymeless H2O2 detection, Nano Res. 8 (2) (2015) 469–480.
[31] S. Cui, L. Li, Y. Ding, J. Zhang, Q. Wu, Z. Hu, Uniform ordered mesoporous ZnCo2O4 nanospheres for super-sensitive enzyme-free H2O2 biosensing and glucose biofuel cell applications, Nano Res. 10 (7) (2017) 2482–2494.
[32] M.A. Shenashen, D. Hassen, S.A. El-Safty, H. Isago, A. Elmarakbi, H. Yamaguchi, Axially oriented tubercle vein and X-crossed sheet of N-Co3O4@C hierarchical mesoarchitectures as potential heterogeneous catalysts for methanol oxidation reaction, Chem. Eng. J. 313 (2017) 83–98.
[33] D. Hassen, M.A. Shenashen, S.A. El-Safty, M.M. Selim, H. Isago, A. Elmarakbi, A. El-Safty, H. Yamaguchi, Nitrogen-doped carbon-embedded TiO2 nanofibers as promising oxygen reduction reaction electrocatalysts, J. Pow. Source 330 (2016) 292–303.
[34] H. Gomaa, H. Khalifa, M. Selim, M.A. Shenashen, S. Kawada, A.S. Alamoudi, A. Azzam, A. Alhamid, S.A. El-Safty, Selective, photo-enhanced trapping/detrapping of arsenate anions using mesoporous blobfish head TiO2 monoliths, ACS Sustain. Chem. Eng. (2017), http://dx.doi.org/10.1021/acssuschemeng.7b02766.
[35] N. Akhtar, S.A. El-Safty, M.E. Abdelsalam, M.A. Shenashen, H. Kawarada, Radially oriented nanostrand electrodes to boost glucose sensing in mammalian blood, Biosens. Bioelectron. 77 (2016) 656–665.
[36] N. Akhtar, S.A. El-Safty, M.E. Abdelsalam, H. Kawarada, One-pot fabrication of dendritic NiO@ carbon-nitrogen dot electrodes for screening blood glucose level in diabetes, ADV. Healthcare Mater. 4 (14) (2015) 2110–2119.
[37] M.A. Shenashen, S. Kawada, M.M. Selim, W.M. Morsy, H. Yamaguchi, A.A. Alhamid, N. Ohashi, I. Ichinose, S.A. El-Safty, Bushy sphere dendrites with husk-shaped branches axially spreading out from the core for photo-catalytic oxidation/remediation of toxins, Nanoscale 9 (2017) 7947–7959.
[38] M.A. Shenashen, D. Hassen, S.A. El-Safty, M.M. Selim, N. Akhtar, A. Chatterjee, A. Elmarakbi, Mesoscopic fabric sheet racks and blocks as catalysts with efficiently exposed surfaces for methanol and ethanol electrooxidation, Adv. Mater. Interfaces 3 (24) (2016), http://dx.doi.org/10.1002/admi.201600743.
[39] M.A. Shenashen, N. Akhtar, M.M. Selim, W.M. Morsy, H. Yamaguchi, S. Kawada, A.A. Alhamid, N. Ohashi, I. Ichinose, A.S. Alamoudi, S.A. el-Safty effective, low cost recovery of toxic arsenate anions from water using hollow sphere trapper geodes, Chem. – Asian J. 12 (15) (2017) 1952–1964.
[40] Y. Li, B.C. Zhang, X.W. Xie, J.L. Liu, Y.D. Xu, W.J. Shen, Novel Ni catalysts for methane decomposition to hydrogen and carbon, J. Catal. 238 (2006) 412–424.
[41] M.A. Shenashen, A. Sherif El-Safty, M. Khairy, Trapping of biological macromolecules in the three-dimensional mesocage pore cavities of monolith adsorbents, J. Por. Mater. 20 (4) (2013) 679–692.
[42] W. Warkocki, S.A. El-Safty, M.A. Shenashen, E. Elshehy, H. Yamaguchi, N. Akhtar, Photo-induced recovery, optical detection, and separation of noxious SeO_3^{2-} using a mesoporous nanotube hybrid membrane, J. Mater. Chem. A 3 (2015) 17578–17589.
[43] M.A. Shenashen, Sherif A. El-Safty, E.A. Elshehy, Monolithic scaff; ;olds for highly selective ion sensing/removal of Co(II), Cu(II), and Cd(II) ions in water, Analyst 139 (24) (2014) 6393–6405.
[44] X. Zhang, W. Shi, J. Zhu, W. Zhao, J. Ma, S. Mhaisalkar, T. Maria, Y. Yang, H. Zhang, H. Hng, Q. Yan, Synthesis of porous NiO nanocrystals with controllable surface area and their application as supercapacitor electrodes, Nano Res. 3 (2010) 643–652.
[45] K. Zhuo, M.-G. Jeong, C.-H. Chung, Dendritic nanoporous nickel oxides for a supercapacitor prepared by a galvanic displacement reaction with chlorine ions as an accelerator, RSC Adv. 3 (2013) 12611–12615.
[46] H.M. Shiri, M. Aghazadeh, Synthesis, characterization and electrochemical properties of capsule-Like NiO nanoparticles, J. Electrochem. Soc. 159 (2012) E132–E138.
[47] M.A. Shenashen, S. Kawada, M.M. Selim, W.M. Morsy, H. Yamaguchi, A.A. Alhamid, N. Ohashi, I. Ichinose, S.A. El-Safty, Bushy sphere dendrite with husk-shaped branches axially spreading out from its core for photo-catalytic oxidation/remediation of toxins, Nanoscale 9 (2017) 7947–7959.
[48] F. Garcia-Garcia, P. Salazar, F. Yubero, A. González-Elipe, Non-enzymatic glucose electrochemical sensor made of porous NiO thin films prepared by reactive magnetron sputtering at oblique angles, Electrochim. Acta 201 (2016) 38–44.
[49] K. Ghanbari, F. Ahmadi, NiO hedgehog-like nanostructures/Au/polyaniline nanofibers/reduced graphene oxide nanocomposite with electrocatalytic activity for non-enzymatic detection of glucose, Analy. Biochem 518 (2017) 143–153.
[50] H. Karimi-Maleh, A.L. Sanati, V.K. Gupta, M. Yoosefian, M. Asif, A. Bahari, A voltammetric biosensor based on ionic liquid/NiO nanoparticle modified carbon paste electrode for the determination of nicotinamide adenine dinucleotide (NADH), Sens. Actuators B 204 (2014) 647–654.
[51] G. Kaur, M. Tomar, V. Gupta, Realization of a label-free electrochemical immunosensor for detection of low-density lipoprotein using NiO thin film, Biosens. Bioelectron. 80 (2016) 294–299.
[52] M.J. Reymond, S.G. Speciale, J.C. Porter, Dopamine in plasma of lateral and medial hypophyseal portal vessels-Evidence for regional variation in the release of hypothalamic dopamine into hypophyseal portal blood, Endocrinology 112 (6) (1983) 1958–1963.